Biomaterials 32 (2011) 4885–4895

Contents lists available at ScienceDirect

Biomaterials

journal homepage: www.elsevier.com/locate/biomaterials

The intrinsic redox reactions of polyamic acid derivatives and their application in hydrogen peroxide sensor

Mu-Yi Hua [a,1,*], Hsiao-Chien Chen [a,1], Cheng-Keng Chuang [b,1], Rung-Ywan Tsai [c], Jyh-Long Jeng [d], Hung-Wei Yang [a], Yaw-Terng Chern [d,**]

[a] Biosensor Group, Biomedical Center, Chang Gung University, 259 Wen-Hwa 1st Rd., Kuei-Shan, Tao-Yuan 33302, Taiwan, ROC
[b] Department of Urology, Chang Gung University College of Medicine and Memorial Hospital, No. 5 Fushing Rd., Tao-Yuan, Taipei 33305, Taiwan, ROC
[c] Electronics and Optoelectronics Research Laboratories, Industrial Technology Research Institute, 195, Sec. 4, Chung-Hsing Rd., Hsin-chu 31040, Taiwan, ROC
[d] Department of Chemical Engineering, National Taiwan University of Science and Technology, 43, Sec. 4, Keelung Rd., Taipei 10607, Taiwan, ROC

ARTICLE INFO

Article history:
Received 28 January 2011
Accepted 21 March 2011
Available online 14 April 2011

Keywords:
Polyamic acid
Hydrogen peroxide
Enzyme-free
Biosensor
Benzothiazole
Benzoxazole

ABSTRACT

Polyamic acids (PAAs) containing benzothiazole (BT) and benzoxazole (BO) pendent groups (PAA-BT and PAA-BO, respectively) which possessed electroactivity were synthesized successfully. The addition of H_2O_2 chemically oxidized the intrinsic carboxylic acid groups of PAA to form peroxy acid groups, and the peroxy acid further oxidized the electroactive sites of BT and BO to form *N*-oxides. The *N*-oxides could be reverted to their original form by electrochemical reduction, thus increasing the electrochemical reductive current. Based on this mechanism, enzyme-free hydrogen peroxide (H_2O_2) biosensors were prepared by modifying gold electrodes with the PAA derivatives (PAA-BT/Au and PAA-BO/Au, respectively). These biosensors had rapid response times (3.9–5.2 s) and high selectivity and sensitivity (280.6–311.2 μA/mM-cm^2). A comparison of the PAA-BT/Au and PAA-BO/Au electrodes with electrodes prepared using polyamide-BT or polyamide-BO (i.e., lacking the carboxylic acid groups) confirmed the mechanism by which PAA derivatives detect H_2O_2. Modifying the surface morphology of the electrode from a planar to a three-dimensional (3D) configuration enhanced the performance of the PAA-BO/Au electrode. The sensitivity of the 3D-PAA-BO/Au electrode was 1394.9 μA/mM-cm^2, ~4.5 times higher than that of the planar electrode. The detection limit was also enhanced from 5.0 to 1.43 μM. The biosensor was used analytically to detect and measure H_2O_2 in urine samples collected from healthy individuals and patients suffering from noninvasive bladder cancer. The results were promising and comparable to that measured by a classical HPLC method, which verified the developed biosensor had a potential to provide a usefully analytical approach for bladder cancer.

1. Introduction

Hydrogen peroxide (H_2O_2) is a reactive oxygen species and a by-product of several types oxidative metabolism [1,2] that easily forms hydroxyl radicals in the presence of transition metals such as iron or copper [3]. At suitable concentrations, such reactive oxygen species are useful for killing bacteria and viruses entering the body. In excess, however, they can damage biological macromolecules such as DNA, carbohydrates or proteins. The relationship between H_2O_2 concentrations and human physiology has thus attracted intensive study [4,5].

Because the accurate determination of H_2O_2 is of practical importance in the clinical, environmental and industrial fields, increasing interest has focused on the fabrication of reliable H_2O_2 biosensors [6–9]. Because of their high selectivity and sensitivity, electrochemical methods have been used extensively to detect H_2O_2 [9]. Biosensors have been fabricated using enzymes or proteins such as horseradish peroxidase (HRP) [9], myoglobin [10] or hemoglobin [11]. However, enzyme-based biosensors lack long-term stability [10], and there have been extensive efforts to develop enzyme-free sensors [12–23]. The simplest method is to electrocatalyze H_2O_2 directly at working potentials of 0.5–0.7 V (Ag/AgCl) [12]. Unfortunately, interfering species such as uric acid (UA) and ascorbic acid (AA) are also electrocatalyzed at these potentials, considerably reducing selectivity. A useful strategy to overcome such interference is to measure H_2O_2 at lower potentials. Electrodes modified with inorganic and organic–inorganic

* Corresponding author. Tel.: +88 63 211 8800x5289; fax: +88 63 211 8668.
** Corresponding author. Tel.: +88 62 2737 6646; fax: +88 62 2737 6644.
E-mail addresses: huamy@mail.cgu.edu.tw (M.-Y. Hua), ytchern@mail.ntust.edu.tw (Y.-T. Chern).
[1] M.-Y. Hua, H.-C. Chen, and C.-K. Chuang contributed equally to this work.

0142-9612/$ – see front matter © 2011 Elsevier Ltd. All rights reserved.
doi:10.1016/j.biomaterials.2011.03.051

materials — metallic particles (Ag, Au, Co, and CuS, nanoparticles) [13–16], metallic oxides (Cu_2O and CuO) [17,18], or transition metals (Prussian Blue and metalloporphyrins) [19,20] — provide stability and convenience of electron transfer. However, only a few studies used polymer-modified electrodes to detect H_2O_2 non-enzymatically at lower potentials [21,22]; incorporating carbon nanotubes and/or gold enhanced the surface area, electrocatalytic activity, and conductivity of such probes [22].

Aromatic polyimides have excellent thermal stability, good chemical resistance, mechanical strength, and low dielectric constants [23]. They are used widely in the microelectronic, aviation, liquid crystal display, and separation industries. However, aromatic polyimides are difficult to process because they are insoluble in most organic solvents and do not flow below their decomposition temperatures. Polyamic acids (PAAs) containing amide and carboxylic acid groups are the usual precursor for polyimides. Beyond that, no other application for PAAs has been found.

The imine structure on pyridines can be oxidized by 30% aqueous H_2O_2 in acetic acid to form pyridine *N*-oxides [24]:

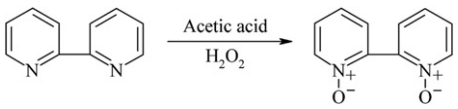

Based on this mechanism, we specifically designed two PAA derivatives containing benzothiazole (BT) and benzoxazole (BO) pendent groups (PAA-BT and PAA-BO, respectively; Fig. 1). The introduction of twisted-biphenyl (2,2′-disubstituted biphenyl) structures decreases polymer packing density and thus increases solubility [25–27]. Incorporating BT or BO pendent groups into PAA therefore significantly increases its solubility, as well as the surface concentration of imine. The carboxylic acid groups of the PAA react with H_2O_2 to form peroxy acid groups, and the imine structures of BT and BO are then oxidized by peroxy acid to form *N*-oxides. The *N*-oxides could be reverted to their original form by electrochemical reduction, resulting in the increase of the electrochemically reductive current.

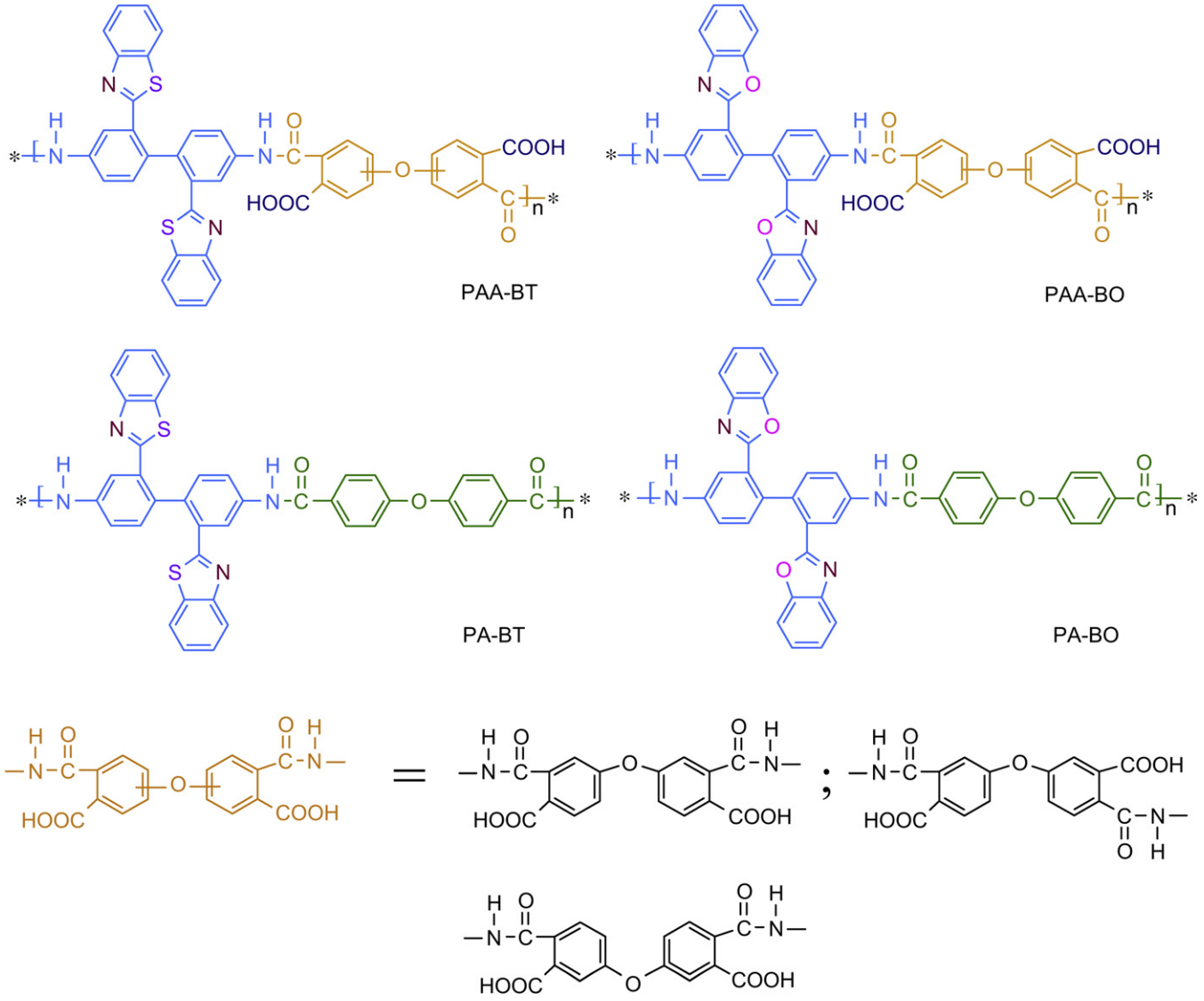

Fig. 1. Chemical structures of PAA-BT, PAA-BO, PA-BT and PA-BO.

2. Materials and methods

2.1. Materials

4,4′-oxydiphthalic anhydride and 4,4′-dicarboxydiphenyl ether were purchased from TCI. H_2O_2, sodium dihydrogen phosphate dihydrate, and disodium hydrogen phosphate were purchased from Showa. *N*,*N*-dimethylacetamide (DMAc), methanol, and 1-methyl-2-pyrrolidone (NMP) were purchased from Tedia. Deionized water was used in all experiments.

2.2. Syntheses of PAA-BT, PAA-BO, PA-BT, and PA-BO

2,2′-bis(2-benzothiazole)-4,4′-diaminobiphenyl (DABPBT) and 2,2′-bis(2-benzoxoazole)-4,4′-diaminobiphenyl (DABPBO) were synthesized as described previously [26,27].

To synthesize PAA-BT, 1.32 mmol of 4,4′-oxydiphthalic anhydride (0.410 g) were added to a stirred solution of DABPBT (0.595 g, 1.32 mmol) in NMP (15% [w/v]) under N_2 for 6 h at room temperature. PAA-BO was similarly prepared by adding 2.06 mmol 4,4′-oxydiphthalic anhydride (0.638 g) to a stirred solution of DABPBO (0.862 g, 2.06 mmol). At a concentration of 0.5 g/dL in NMP at 30 °C, the inherent viscosities of the PAA-BT and the PAA-BO were 1.21 dL/g and 1.02 dL/g, respectively.

The polyamide (PA) derivatives PA-BT and PA-BO were prepared by mixing 0.5 mmol of DABPBT (0.225 g) or DABPBO (0.209 g), respectively, with 0.129 g of 4,4′-dicarboxydiphenyl ether, 0.1 g of calcium chloride, 0.6 mL of triphenyl phosphite, 0.2 mL of pyridine, and 2.0 mL of NMP. The polymer solutions were heated with stirring at 120 °C for 4 h, then poured slowly into 200 mL of stirring methanol. The stringy precipitate was collected by filtration, washed thoroughly with hot water and methanol, and dried at 120 °C. Further purification was performed by reprecipitation twice from DMAc into methanol. At a concentration of 0.5 g/dL in NMP at 30 °C, the inherent viscosities of PA-BT and PA-BO were 1.45 dL/g and 0.96 dL/g, respectively.

2.3. Chemical oxidation of PAA-BT and PAA-BO

Two hundred micromoles of PAA-BT or PAA-BO were dissolved in 10 mL of NMP and added to 2 mL of 0.5 M H_2O_2. The reactions were incubated in a 43-kHz ultrasonic bath at 40 °C for 0.5 h in a dark room. Samples were centrifuged at 5500 rpm for 15 min and the precipitates were washed three times with acetone before drying in a vacuum aspirator at 80 °C for one day.

2.4. Preparation of PAA-BT/Au, PAA-BO/Au and 3D-PAA-BO/Au electrodes

To prepare PAA-BT or PAA-BO modified Au (PAA-BT/Au or PAA-BO/Au) electrode, 0.05 g of PAA-BT or PAA-BO was dissolved in 3 mL of NMP. One μL of each solution was dropped onto an Au disk electrode (0.196 cm^2) and dried in a vacuum aspirator at 50 °C for 5 h.

To prepare the three-dimensional PAA-BO modified Au (3D-PAA-BO/Au) electrode, 0.05 g of PAA-BO was dissolved in 3 mL of NMP and precipitated into 50 mL of stirred acetone. After centrifugation at 5500 rpm, the precipitate was washed three times with acetone. The final precipitate was dispersed into 3 mL acetone, and 1 μL of the solution was dropped onto an Au disk electrode (0.196 cm^2) and dried in a vacuum aspirator at 50 °C for 5 h.

2.5. Equipment and measurements

Fourier transform infrared (FT-IR) spectra were obtained using a Bruker-Tensor 27 spectrometer at a spectral resolution of 8 cm^{-1}. X-ray photoelectron spectroscopy (XPS) measurements were performed using a VG Scientific ESCALAB 250 system. Field-emission scanning electron microscopy (FE-SEM) was performed using a Hitachi S-5000 system. Electrochemical measurements were performed on a CHI 660A electrochemical workstation (CH Instruments, USA) with a three-electrode system consisting of the PAA-BT/Au or PAA-BO/Au electrode, a bare Au electrode, and an Ag/AgCl electrode as the working, counter, and reference electrodes, respectively. All electrochemical measurements were performed in 40 mL of 0.2 M phosphate buffer solution (PBS) at 25 °C. The pH values were adjusted with acetic acid. Proton nuclear magnetic resonance (^{1}H NMR) spectra were measured on a Bruker AVANCE-500 FT-NMR using tetramethylsilane as the internal standard.

3. Results and discussion

3.1. Characterization of PAA-BT, PAA-BO, PA-BT and PA-BO

The FT-IR spectra of PAA-BT and PAA-BO (Fig. 2a,b) both showed absorptions at 3300 cm^{-1} (N–H and O–H stretching) and 1722 cm^{-1} and 1670 cm^{-1} (C=O stretching) characteristics of amic acid [28]. In contrast, the FT-IR spectra of PA-BT and PA-BO displayed characteristic amide absorption bands at 3297 cm^{-1} (N–H stretching) and 1662 cm^{-1} (amide carbonyl) (Fig. 2c,d).

^{1}H NMR of PAA-BT performed in DMSO-d_6 detected chemical shifts at 7.23–7.60 (10H, H-1,4,5,8,9), 7.82–8.06 (8H, H-2,6,7,10), 8.79 (2H, H-3), and 10.9–11.2 ppm (2H, NH) (Fig. 3a), with a π-π* transition at 298 nm. PAA-BO similarly displayed shifts at 7.23–7.56 (14H, H-1,4,5,7,8,9,10), 7.84–8.06 (4H, H-2,6), and 10.9–11.1 ppm (2H, NH) (Fig. 3b), with a π-π* transition at 292 nm. The ^{1}H NMR spectrum of PA-BT produced shifts at 7.29–7.50 (10H, H-1,5,7,8), 7.95 (4H, H-4), 8.19 (6H, H-2,6,9), 8.86 (2H, H-3), and 10.7 ppm (2H, NH) (Fig. 3c), with a π-π* transition at 294 nm, whereas the spectrum for PA-BO displayed the most complex pattern, with shifts at 7.29–7.32 (8H, H-5,7,8), 7.41 (2H, H-1), 7.47 (2H, H-6), 7.57 (2H, H-9), 8.11–8.19 (6H, H-2,4), 8.68 (2H, H-3), and 10.6 ppm (2H, NH) (Fig. 3d); the π-π* transition was at 298 nm. These results demonstrate the first successful synthesis of PAA-BT and PAA-BO.

3.2. Characterization of PAA-BT and PAA-BO oxides

The chemical synthesis of pyridine *N*-oxides has been reported previously [24]. In 30% aqueous H_2O_2 in acetic acid, pyridines are preferentially *N*-oxidized during the formation of peracetic acid. However, because PAA-BT and PAA-BO possess both carboxylic acid groups and imine structures, oxidation in the presence of H_2O_2 should occur in the absence of acetic acid. Reacting PAA-BT with H_2O_2 did not obviously shift the original FT-IR peaks of PAA-BT (Fig. 2e), although the intensity of the peak at 1268 cm^{-1} was much stronger because of the contribution from *N*-oxide formation [24]:

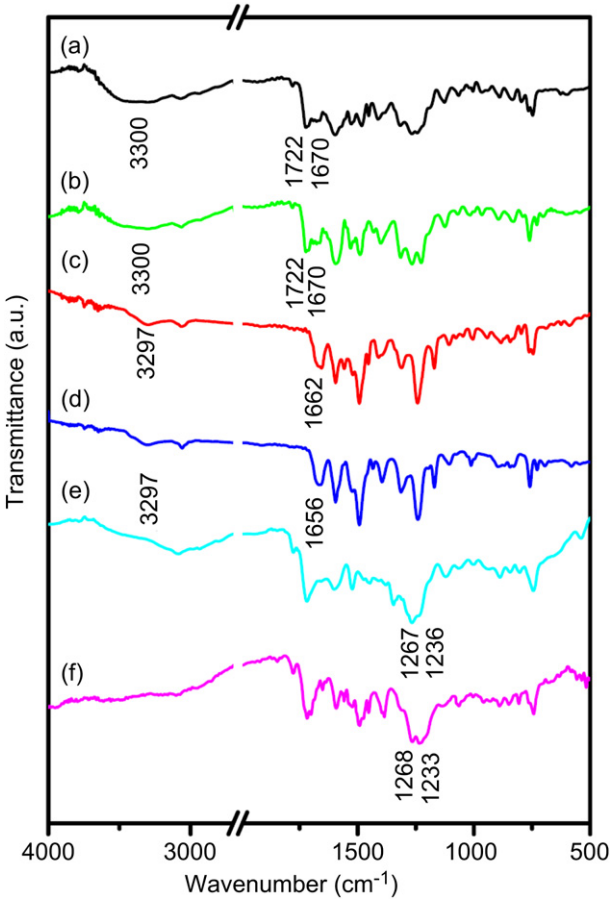

Fig. 2. FT-IR spectra of (a) PAA-BT, (b) PAA-BO, (c) PA-BT, (d) PA-BO, (e) PAA-BT treated with H_2O_2, and (f) PAA-BO treated with H_2O_2.

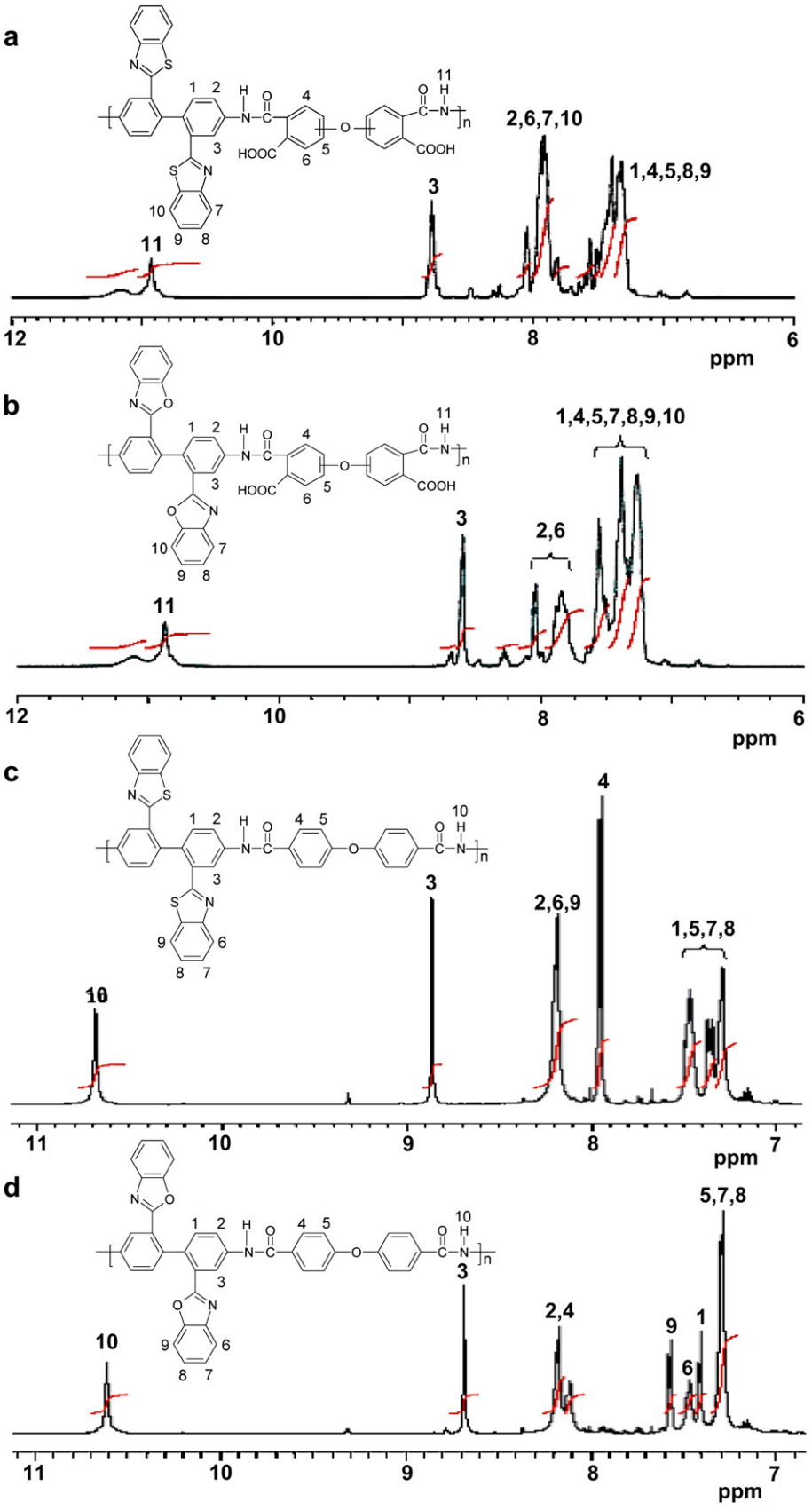

Fig. 3. 1H NMR (500 MHz) spectra of (a) PAA-BT, (b) PAA-BO, (c) PA-BT, and (d) PA-BO.

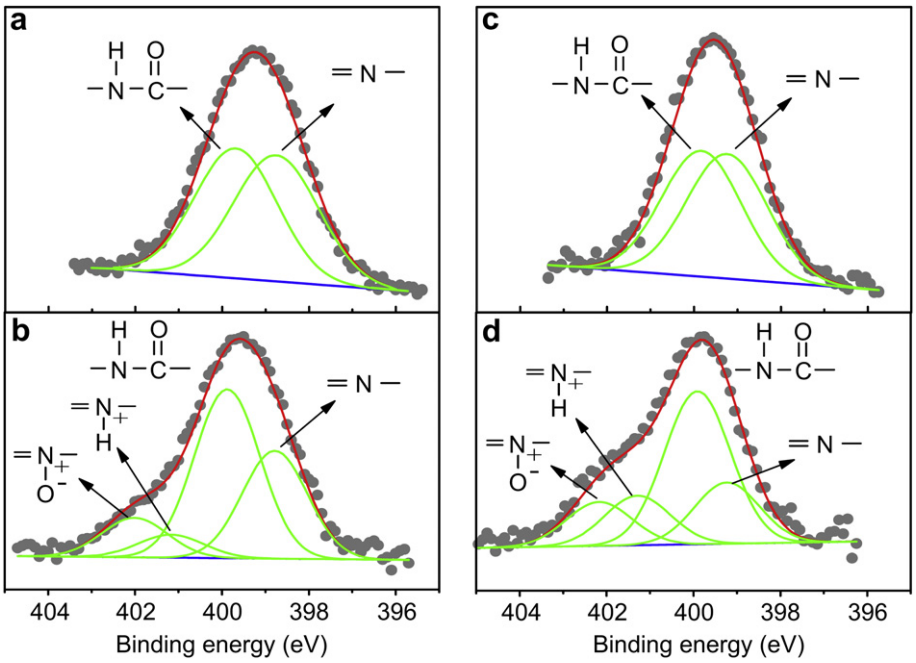

Fig. 4. N(1s) XPS spectra of (a) PAA-BT, (b) PAA-BT *N*-oxide, (c) PAA-BO, and (d) PAA-BO *N*-oxide.

relative to the intensity of the C=O stretching peaks at 1722 and 1670 cm^{-1}, the peak at 1268 cm^{-1} increased 18.6%. Similar results were obtained for PAA-BO (Fig. 2f). The formation of *N*-oxide indicates that the carboxylic acid groups of both polymers could convert to peroxy acids, which then oxidized the polymers at the imine sites, consistent with the results seen in pyridine *N*-oxide formation [24].

PAA-BT, PAA-BO, and their oxides were also characterized by N(1s) XPS (Fig. 4). The spectra of PAA-BT (Fig. 4a) and PAA-BO (Fig. 4c) deconvoluted into two peaks with an area ratio of 1:1: an imine peak at 398.8 eV (PAA-BT) or 399.2 eV (PAA-BO), and an amide peak at 399.8 eV [29,30]. The slightly higher imine binding energy of PAA-BO is likely because the electronegativity of oxygen (3.44) is higher than that of sulfur (2.58). No peaks resulting from the protonation of imines were observed at 401.2 eV, indicating that dissociation of carboxylic groups and protonation of imines did not occur during polymer synthesis. After oxidation of PAA-BT by H_2O_2, the N(1s) spectra deconvoluted into four peaks (Fig. 4b). Two remained at the same positions as those of PAA-BT. The third peak (at 401.2 eV) was the result of imine partially protonated by the carboxylic acid in the solution [31], but the fourth peak (at 402.0 eV) was attributed to *N*-oxide formation [32]. The spectrum for PAA-BO oxide similarly deconvoluted into four peaks (Fig. 4c), although the binding energies for the protonated imine and imine *N*-oxide were 0.1–0.2 eV higher than those for PAA-BT oxide. In contrast, the area of the amide peak remained constant and equal to the sum of the areas of the imine, protonated imine and *N*-oxide peaks, indicating that oxidation occurred only at the imine sites, with 28.2% and 28.8% of the imines of PAA-BT and PAA-BO were oxidized, respectively (Table 1).

Table 1
Ratios of the areas of nitrogen peaks from N(1s) XPS spectra and the degree of oxidation (d_{Ox}) for PAA derivatives.

	–N=	–N–C(=O)–	–N(+)H=	–N(+)(O⁻)=	d_{Ox} [a]
PAA-BT	49.9%	50.1%	—	—	—
PAA-BT *N*-oxide	30.4%	49.9%	5.6%	14.1%	28.2%
PAA-BO	50.1%	49.9%	—	—	—
PAA-BO *N*-oxide	19.8%	50.0%	16.0%	14.4%	28.8%

—: not measured.
[a] d_{Ox} was calculated as the ratio of the *N*-oxide peak to the sum of the areas of the imine, protonated imine, and *N*-oxide peaks.

3.3. Electrochemical behaviors of the PAA-BT/Au and PAA-BO/Au electrodes

Relative to an unmodified Au electrode, the electrochemical behaviors of PAA-BT/Au and PAA-BO/Au electrodes in 0.2 M PBS (pH 7.0) were markedly different, suggesting that the electrodes were overcoated with polymers (Fig. 5). Cyclic voltammograms (CVs) of the PAA-BT/Au electrode showed anodic (E_{pa}) and cathodic (E_{pc}) peak potentials characteristic of electroactive imines at 0.02 V and −0.23 V (Fig. 5b). The formal potential ($E^{0'}$, defined as the average of E_{pa} and E_{pc}) was −0.11 V, and the peak-to-peak separation (ΔE_p) was 0.25 V. The PAA-BO/Au electrode also displayed redox

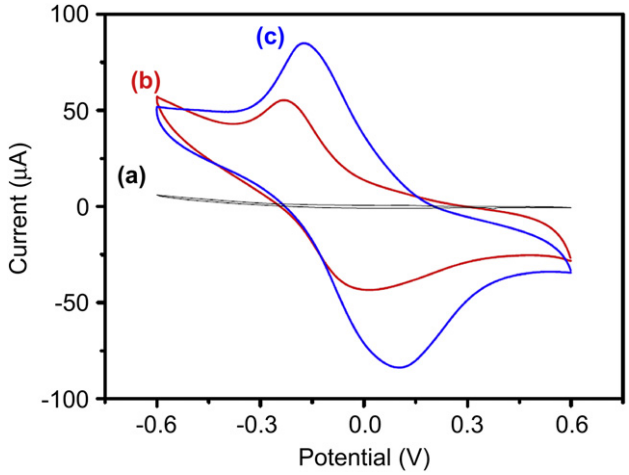

Fig. 5. CVs of electrodes in 0.2 M PBS (pH 7.0) at a scan rate of 0.1 V/s: (a) bare Au electrode, (b) PAA-BT/Au electrode, and (c) PAA-BO/Au electrode.

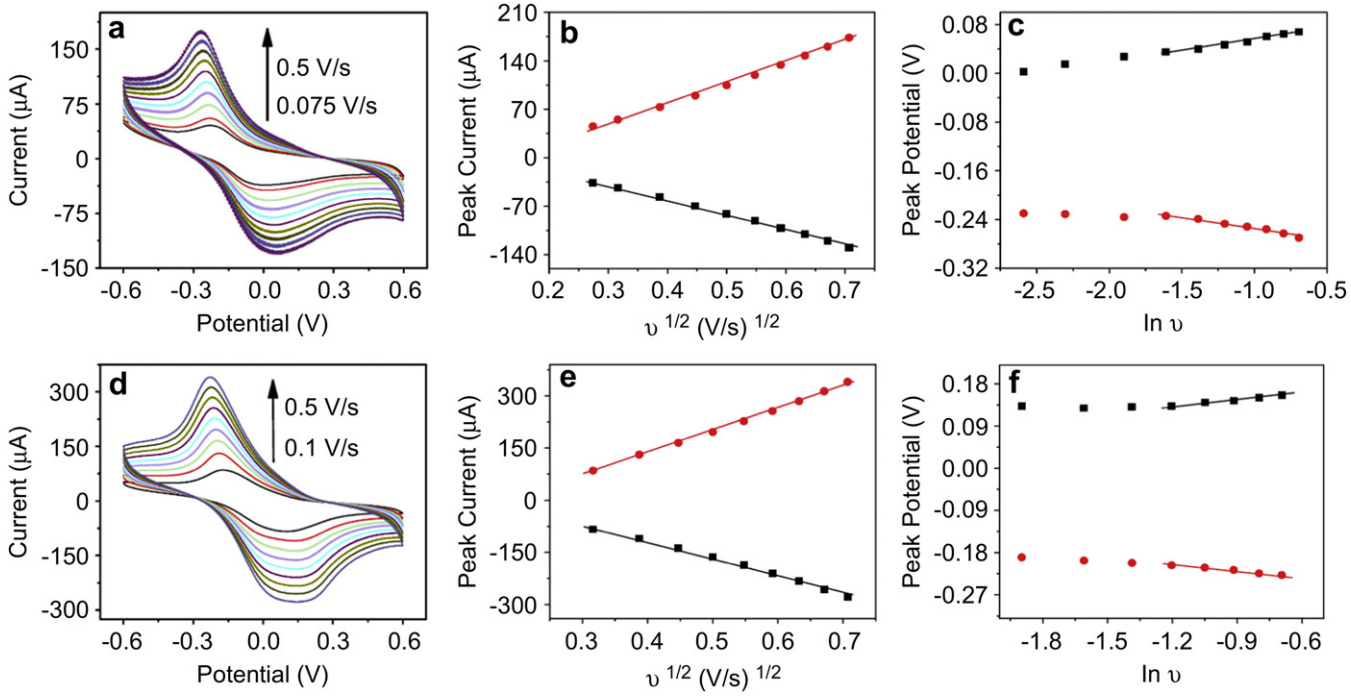

Fig. 6. (a) and (d): CVs of electrodes in 0.2 M PB (pH 7.0) at various scan rates (υ): (a) PAA-BT/Au electrode, (d) PAA-BO/Au electrode. (b) and (e): Linear relationships of peak current vs. $\upsilon^{1/2}$ for the (b) PAA-BT/Au and (e) PAA-BO/Au electrodes. (c) and (f): Linear relationships of peak potential vs. lnυ, for the (c) PAA-BT/Au and (f) PAA-BO/Au electrodes.

peaks at 0.10 V (E_{pa}) and −0.17 V (E_{pc}) with an $E^{0'}$ of −0.04 V (Fig. 5c). The anodic peak of PAA-BO/Au was distinctly higher than that of PAA-BT/Au, indicating that, in accordance with the XPS analyses, the electron at the imine site of PAA-BO/Au was not easy to lose.

To understand further the kinetics of the electron transfer process, the effects of varying the scan rate (υ) on the peak currents and peak potentials of both electrodes were evaluated. For the PAA-BT/Au electrode, the peak current increased along with the υ from 0.075 to 0.5 V/s (Fig. 6a). Furthermore, the peak currents of the electroactive imines increased linearly with the square root of the υ (Fig. 6b), characteristic of a diffusion-controlled process [33]. The peak-to-peak separation also increased slightly as υ increased, and this tended to be more irreversible, presumably because the low conductivity of the polymer increased the resistance of the electrode. When $\upsilon > 0.2$ V/s, the peak potentials were proportional to the natural logarithm of υ (Fig. 6c). Similar results were observed for the PAA-BO/Au electrode (Fig. 6d–f). The redox peak potentials were $E_{pa}(V) = 0.101 + 0.043\ \ln\upsilon$ and $E_{pc}(V) = -0.292 - 0.037\ \ln\upsilon$ for the PAA-BT/Au electrode and $E_{pa}(V) = 0.187 + 0.045\ \ln\upsilon$ and $E_{pc}(V) = -0.257 - 0.043\ \ln\upsilon$ for the PAA-BO/Au electrode. Furthermore, the electrochemical reactions on the modified electrode surfaces in PBS were irreversible when the $\Delta E_p > 0.2$ V. For such an irreversible reaction, the parameters of the electrochemical reaction can be calculated:

$$E_{pa} = E^{0'} - \frac{RT}{(1-\alpha)n\mathrm{F}}\ln\frac{RTk_s}{(1-\alpha)n\mathrm{F}} + \frac{RT}{(1-\alpha)n\mathrm{F}}\ln\upsilon$$

$$E_{pc} = E^{0'} + \frac{RT}{\alpha n\mathrm{F}}\ln\frac{RTk_s}{\alpha n\mathrm{F}} - \frac{RT}{\alpha n\mathrm{F}}\ln\upsilon$$

where α is the electron transfer coefficient, n is the electron transfer number, F is the Faraday's constant, k_s is the electron transfer rate constant, R is 8.314 J/mol-K, and T is the absolute temperature (298 K) [34,35]. The plots of E_{pa} and E_{pc} versus lnυ yield two straight lines whose slopes, k_a and k_c, are equal to $RT/(1-\alpha)n\mathrm{F}$ and $-RT/\alpha n\mathrm{F}$. The value of α can be determined:

$$\alpha = k_a/(k_a - k_c)$$

The values of α were 0.55 and 0.51 for the PAA-BT/Au and PAA-BO/Au electrodes, respectively. The numbers of electron involved in the redox reactions (n) were 1.33 and 1.17, for PAA-BT and PAA-BO, respectively; both values approached 1, indicative of a single electron transfer at the imines.

The surface concentration (Γ) of electroactive imines could also be calculated [36]:

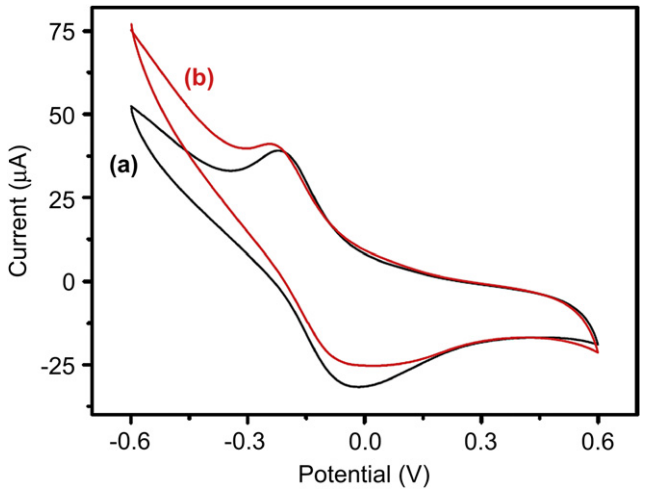

Fig. 7. CVs of the PAA-BT/Au electrode in the (a) absence and (b) presence of 1 mM H_2O_2.

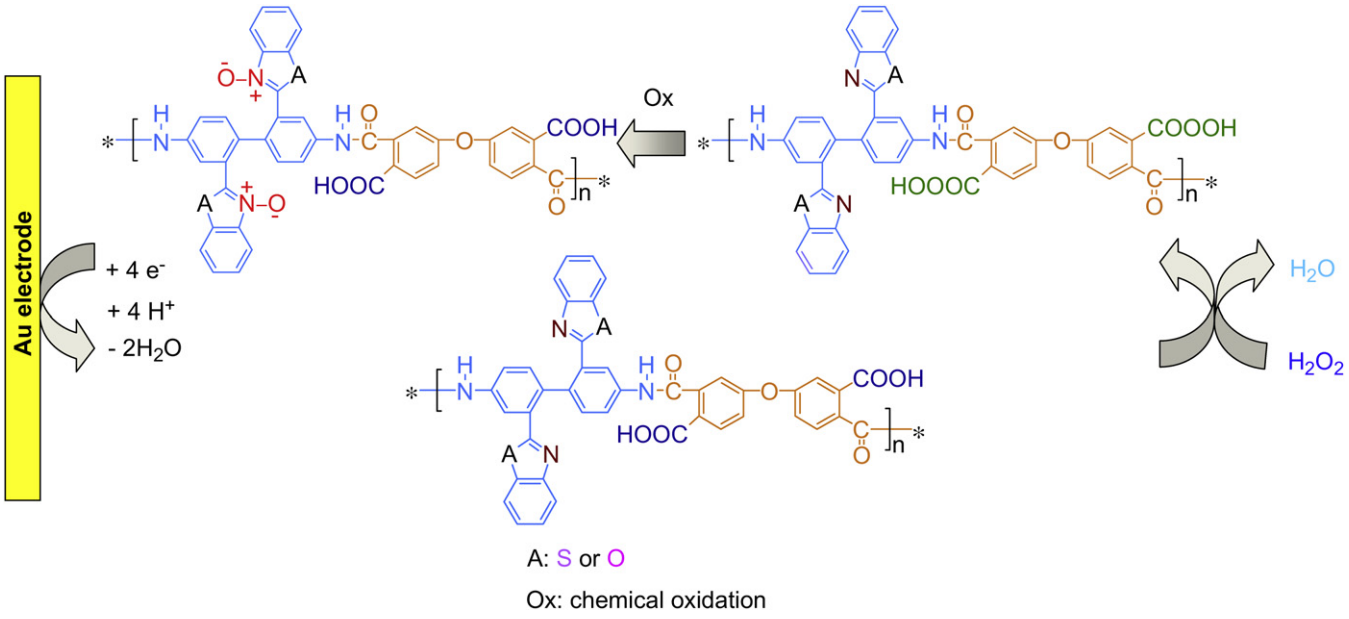

Scheme 1. The mechanism for H_2O_2 detection by PAA-BT/Au and PAA-BO/Au electrodes.

$$I_p = \left(n^2F^2\upsilon A\Gamma\right)/4RT,$$

where υ is the potential sweep rate and A is the electrode surface area (0.196 cm^2). The Γ of electroactive imines on the PAA-BT/Au electrode was 1.39×10^{-9} mol/cm^2. Interestingly, the Γ of the PAA-BO/Au electrode was higher (3.47×10^{-9} mol/cm^2), possibly because PAA-BO is more hydrophilic than PAA-BT, resulting in a higher affinity for PBS during the electrochemical reaction (the contact angles with PBS were 64.8° for PAA-BT and 55.5° for PAA-BO).

For enzymatic biosensors, the concentration and activity of the enzyme are the main factors influencing the surface reactivity of electroactive species. Biosensor performance can be enhanced by immobilizing enzymes on the modified electrode with a three-dimensional morphology to increase the concentrations of electroactive sites [33,37]. Nevertheless, steric hindrance can limit the quantity of enzyme that can be applied. In the present study, the number of electroactive imines on the surface of modified electrode is the most important indicator of activity, and unlike macromolecular enzymes, there are two reactive imines for each repeating unit along the polymer chain; presumably, there is an equal concentration of chemically reactive carboxylic acid groups that can be oxidized by H_2O_2 to form peroxy acid. Furthermore, the PAA-BT/Au and PAA-BO/Au electrodes were designed to decrease the

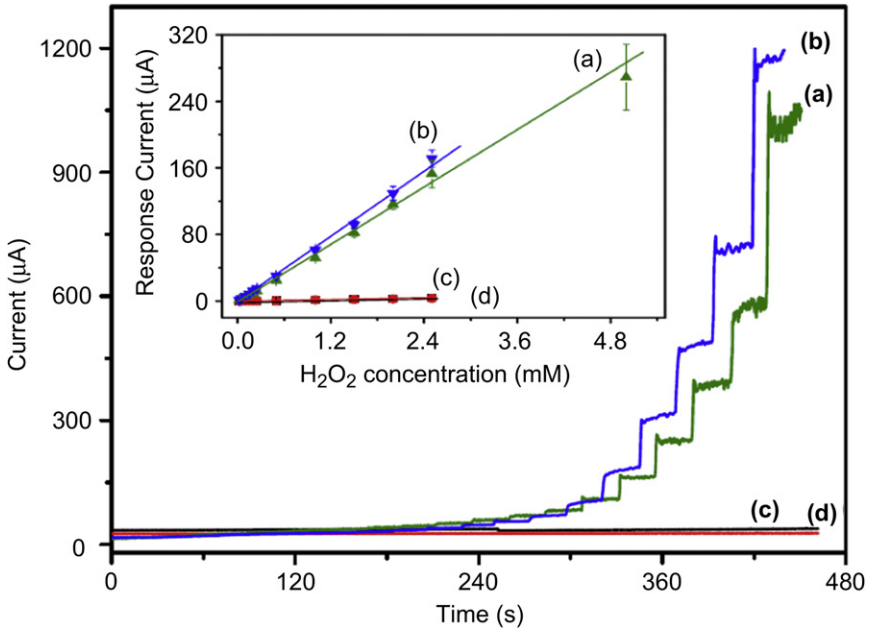

Fig. 8. Current–time plots of (a) PAA-BT/Au, (b) PAA-BO/Au, (c) PA-BT/Au, and (d) PA-BO/Au electrodes after successive addition of increasing concentrations of H_2O_2. Inset: Linear dependence of response currents vs. H_2O_2 concentration ($n = 5$).

Table 2
Performance parameters of H_2O_2 biosensors based on PAA-derivative-modified Au electrodes.

	Sensitivity ($\mu A/mM\text{-}cm^2$)	Linear Range (mM)	Detection Limit(μM)	Response Time (s)	R	Relative St. Dev. (%)
PAA-BT/Au	280.6	0.025–5.0	4.9	5.2	0.997	3.9
PAA-BO/Au	311.2	0.025–2.5	5.0	3.9	0.998	4.1
3D-PAA-BO/Au	1394.9	0.00625–2.5	1.4	1.9	0.997	3.7

packing densities of the polymers, thus increasing the surface concentrations of electroactive imines.

3.4. Characterization of H_2O_2 biosensors based on PAA-BT/Au and PAA-BO/Au electrodes

The above results indicate that PAA-BT and PAA-BO polymers can be oxidized by H_2O_2 at imine sites. In addition, they also show the redox reaction during electrochemical process. Therefore, it would be practical to develop H_2O_2 biosensor based on these polymers. In the presence of 1 mM H_2O_2, there was a significant increase in reduction current whereas the oxidation peak current decreased, indicating that chemical oxidation occurred automatically (Fig. 7b). This behavior is similar to H_2O_2 biosensors based on HRP where the enzyme is oxidized by H_2O_2 and then reduced electrochemically to its native state by accepting two electrons [38]. Accordingly, we propose a three-step mechanism (Scheme 1) by which the enzyme-free PAA-BT/Au electrode detects H_2O_2. Adding H_2O_2 chemically oxidizes the carboxylic acid groups to form peroxy acid, which then chemically oxidize imines to form imine *N*-oxide. Finally, each *N*-oxide reverts to an imine by accepting two electrons and two protons during electrochemical reduction.

In the presence of 1 mM H_2O_2, the response current of the PAA-BT/Au electrode increased over the range from −0.2 to −0.6 V (Fig. 7). To ensure the reductive reaction went to completion and to maintain the equilibrium of the response current, an applied potential of −0.5 V (i.e., more negative than the reduction peak at −0.23 V) was used for further experiments. As expected, when the concentration of H_2O_2 was increased by successive addition of H_2O_2 in PBS (pH 7.0) at a stirrer rotation speed of 400 rpm, the response currents of the PAA-BT/Au electrode increased (Fig. 8a). The electrode response was rapid and sensitive, reaching ~95% of the steady-state current less than 5.2 s after each addition of H_2O_2. The current response to H_2O_2 was linear over a range from 25 μM to 5 mM ($R = 0.997$), with a sensitivity of 280.6 $\mu A/mM\text{-}cm^2$ (Fig. 8a, inset; Table 2). The detection limit was 4.9 μM at a signal-to-noise ratio of 3. Under the same conditions, the response time of the PAA-BO/Au electrode was less than 3.9 s, and its response to H_2O_2 was linear over a range from 25 μM to 2.5 mM with a sensitivity of 311.2 $\mu A/mM\text{-}cm^2$ (Fig. 8b; Table 2). The higher sensitivity of the PAA-BO/Au electrode is likely the result of the higher affinity of PBS and the resulting higher concentration of reactive imine, rather than the higher oxidative potential noted by the XPS analysis. In contrast, the negligible response currents of PA-BT/Au and PA-BO/Au electrodes (i.e., lacking carboxylic acid groups) demonstrate that they were hardly to be oxidized by H_2O_2 in the absence of carboxylic acid groups. On the other hand, it has been reported that enzyme-free H_2O_2 biosensor was sensitive with oxygen production during the H_2O_2 reduction at negative potentials [13]. In this study, no response currents for PA-BT/Au and PA-BO/Au electrodes in the presence of H_2O_2 were obtained, indicating that H_2O_2 were not reduced to oxygen by PA-BT/Au and PA-BO electrodes. Thus, it is confirmed that the generated response currents after addition of H_2O_2 were according to the mechanism proposed in Scheme 1.

3.5. Effects of interfering compounds on biosensor responses

Other substances such as UA and AA can interfere with the electrochemical reduction of H_2O_2. However, the potentials to oxidize AA and UA directly occur at 0.25 and 0.54 V, respectively [39]. Because the detection processes of the PAA-BT/Au and PAA-BO/Au electrodes were applied at negative potential that can avoid such interference, addition of AA and/or UA had no effect on the current responses to H_2O_2 (Fig. 9a,b), indicating that these biosensors were highly selective.

3.6. Characterization of the H_2O_2 biosensor based on 3D-PAA-BO/Au electrode

The above results indicated that reliable H_2O_2 biosensors based on PAA-BT/Au and PAA-BO/Au electrodes were feasible, although the sensitivity was limited. To improve biosensor performance, the morphology of the PAA-BO/Au electrode surface was modified from

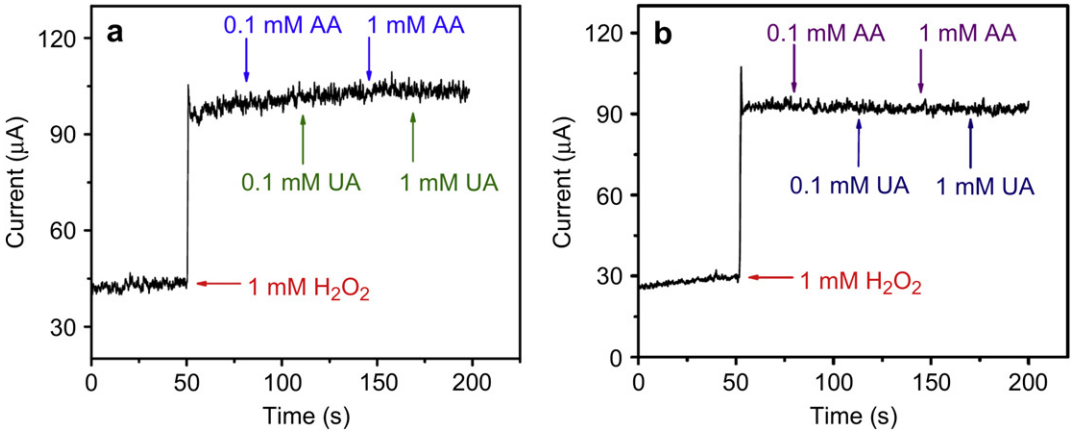

Fig. 9. Effects of interfering species on the response currents of (a) PAA-BT/Au and (b) PAA-BO/Au electrodes to 1 mM H_2O_2.

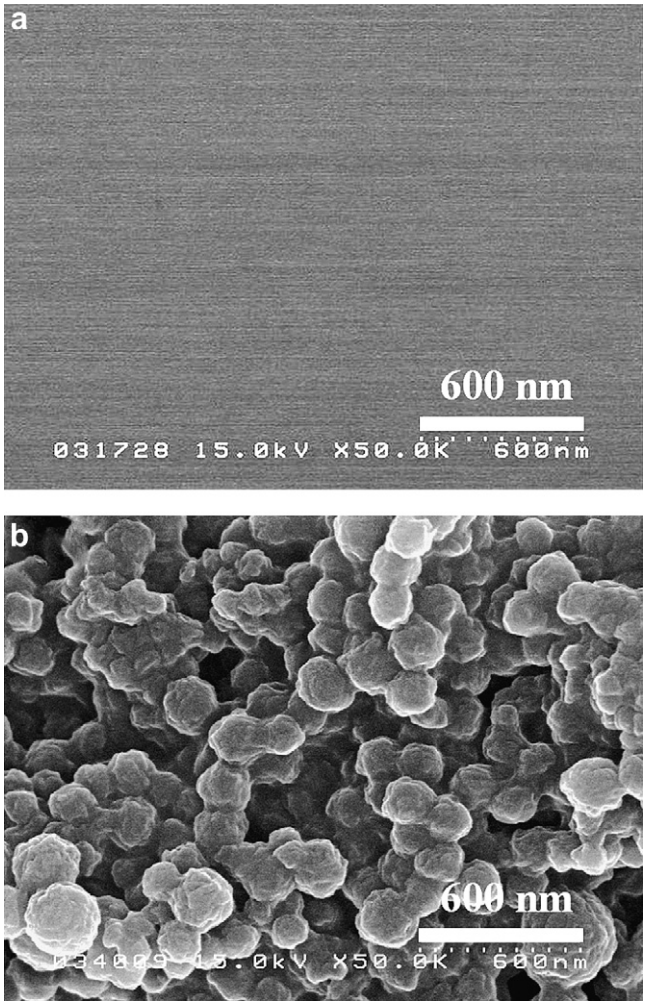

Fig. 10. Scanning electron micrographs of (a) PAA-BO/Au and (b) 3D-PAA-BO/Au electrodes.

a planar (Fig. 10a) to a three-dimensional structure (Fig. 10b). By mixing the polymer solution with acetone, the polymer chains become entangled and remain suspended in the solvent. When this is applied to the Au electrode surface the aggregation of PAA-BO particles forms a granular three-dimensional structure (Fig. 10b). At an applied potential of −0.5 V, the 3D-PAA-BO/Au electrode showed a rapid response time, reaching ~95% of the steady-state current in ~1.9 s (Fig. 11a) presumably because the H_2O_2 could diffuse through the granulated surface freely [40]. The 3D electrode's response to H_2O_2 was linear over a range from 6.25 μM to 2.5 mM (Fig. 11b; Table 2). Also, because of the increased surface area, the sensitivity of the 3D-PAA-BO/Au electrode was 1394.9 μA/mM-cm^2, ~4.5 times higher than that of the planar electrode. The detection limit was also enhanced from 5.0 to 1.43 μM.

3.7. Practical application of the H_2O_2 biosensor based on 3D-PAA-BO/Au electrode

H_2O_2 is the product of oxidative stress — a primary mechanism of DNA damage — that could mediate aging and the progression of numerous age-related diseases, including cancer. To assess the utility of the H_2O_2 biosensor based on 3D-PAA-BO/Au electrode for clinical analysis, urine samples were collected from healthy individuals and patients diagnosed with noninvasive bladder cancer ($n = 12$; Fig. 12) after 8 h fasting. The average H_2O_2 concentration in the samples from healthy individuals was ~0.1 mM, whereas the average concentration in the samples from cancer patients was 0.59 mM. In both groups, values detected using the 3D-PAA-BO/Au electrodes were comparable with those obtained using a classical HPLC method of detection.

It should be noted that the PAA-modified biosensor not only responds to free H_2O_2 (via the conversion of carboxylic groups to peroxy acid) but also detects peroxy acid formed by other means, which might account for the consistently higher results obtained by the probe than by HPLC. Various organic acids (e.g., pyruvate, lactate, isocitrate, etc.) in human urine can also form peroxy acid in the presence of H_2O_2, which might reduce its initial concentration in the bladder. However, HPLC measurements using a triphenyl phosphate probe did not identify these substances, suggesting that the PAA-modified electrode might indeed provide a more sensitive

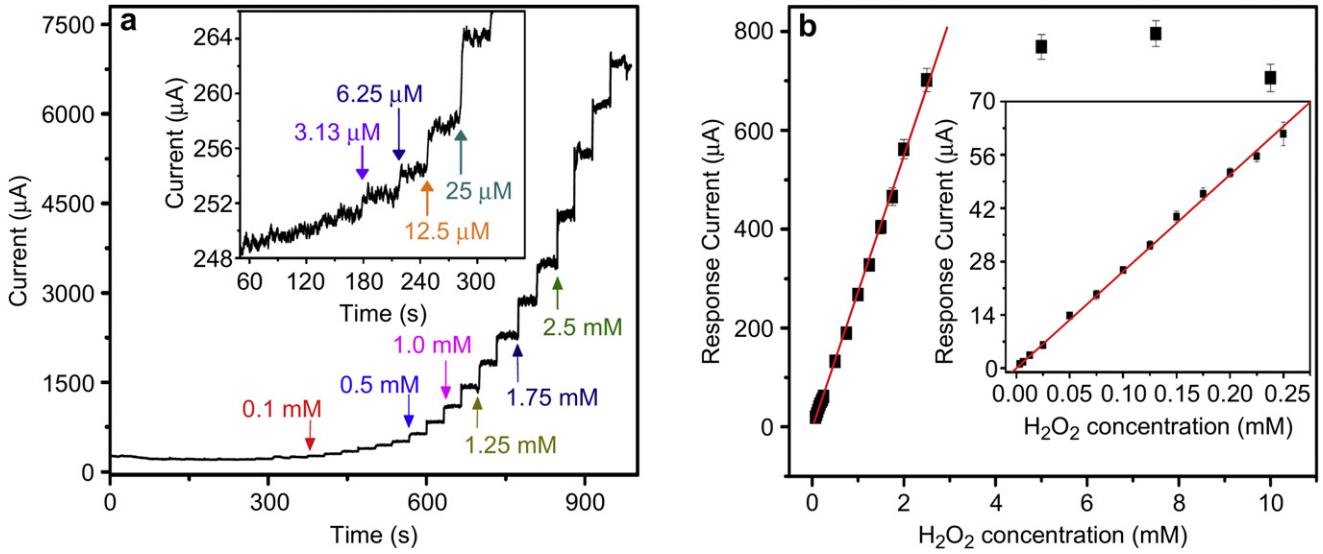

Fig. 11. (a) Current–time plot of the 3D-PAA-BO/Au electrode after the successive addition of increasing concentrations of H_2O_2. Inset: Response current at low concentrations of H_2O_2. (b) Linear dependence of response current vs. H_2O_2 concentration. Inset: Linear dependence of the response current vs. H_2O_2 at low concentrations ($n = 5$).

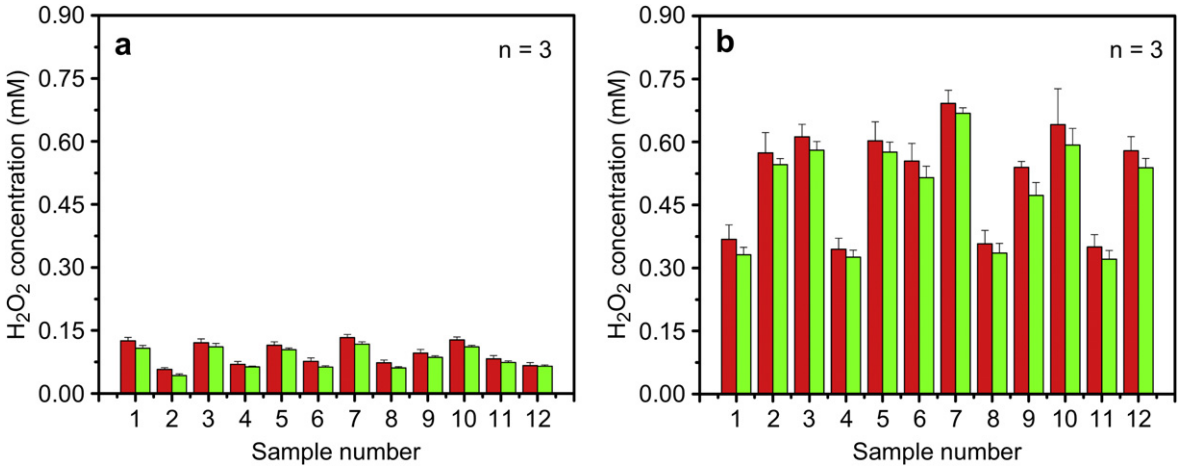

Fig. 12. Detection of H_2O_2 by HPLC (green) and by a 3D-PAA-BO/Au electrode (red) in urine samples from (a) healthy individuals and (b) patients diagnosed with bladder cancer. (For interpretation of the references to colour in this figure legend, the reader is referred to the web version of this article.)

and accurate means of measuring H_2O_2 concentrations in the human body. Investigations into the correlation between the higher H_2O_2 concentrations seen in patients with bladder cancer and the course of medical treatment are currently in progress.

4. Conclusion

This study describes the successful development of PAA-BT/Au and PAA-BO/Au electrodes that can be applied as enzyme-free H_2O_2 biosensors with superior performances. The PAA derivatives possess carboxylic acid groups on the main chain that form peroxy acid groups in the presence of H_2O_2. The imines on the side chains are electroactive and can be oxidized by the peroxy acid groups to form *N*-oxides. The *N*-oxides can be reverted to their original form by electrochemical reduction, resulting in the increase of reductive current. The intrinsic properties of the polymers grant them a higher concentration of electroactive imines as well as greater stability. H_2O_2 biosensors based on PAA-BT/Au and PAA-BO/Au electrodes show rapid response times and high selectivities. The performance of the PAA-BO/Au electrode can be improved further by modifying the surface morphology from a planar to a granular, three-dimensional structure. This combination of easily prepared materials and electrode design provides an enzyme-free means of measuring H_2O_2 with favorable reproducibility, stability, selectivity, and accuracy.

Acknowledgments

We thank the National Science Council of the Republic of China, Chang Gung University and Ministry of Economic Affairs for financial aid: NSC 99-2221-E-182-068, NSC 98-3114-E-182-001-CC2, CGURPD280091, and A356AE1120.

References

[1] Wen Z, Ci S, Li J. Pt nanoparticles inserting in carbon nanotube arrays: nanocomposites for glucose biosensors. J Phys Chem C 2009;113:13482–7.
[2] Li J, Peng T, Peng Y. A cholesterol biosensor based on entrapment of cholesterol oxidase in a silicic sol-gel matrix at a Prussian blue modified electrode. Electroanalysis 2003;15:1031–7.
[3] Macomber L, Rensing C, Imlay JA. Intracellular copper does not catalyze the formation of oxidative DNA damage in *Escherichia coli*. J Bacteriol 2007; 189:1616–26.
[4] Liochev SI, Fridovich I. The role of O_2^- in the production of HO: in vitro and in vivo. Free Radic Biol Med 1994;16:29–33.
[5] Luo Y, Liu H, Rui Q, Tian Y. Detection of extracellular H_2O_2 released from human liver cancer cells based on TiO_2 nanoneedles with enhanced electron transfer of cytochrome *c*. Anal Chem 2009;81:3035–41.
[6] Weber PA, Thomas JE, Skinner WM. Smart RStC. Improved acid neutralisation capacity assessment of iron carbonates by titration and theoretical calculation. Appl Geochem 2004;19:687–94.
[7] Goral VN, Nelen MI, Ryabov AD. Ferrocene and ferricenium ion as versatile photometric titrants of H_2O_2 and *D*-glucose in the presence of peroxidase and glucose oxidase. A ferrocene–peroxidase stairway. Anal Lett 1995;28: 2139–48.
[8] He F, Tang Y, Yu M, Wang S, Li Y, Zhu D. Fluorescence-amplifying detection of hydrogen peroxide with cationic conjugated polymers, and its application to glucose sensing. Adv Funct Mater 2006;16:91–4.
[9] Kafi AKM, Wu G, Chen A. A novel hydrogen peroxide biosensor based on the immobilization of horseradish peroxidase onto Au-modified titanium dioxide nanotube arrays. Biosens Bioelectron 2008;24:566–71.
[10] Esplandiu MJ, Pacios M, Cyganek L, Bartroli J, del Valle M. Enhancing the electrochemical response of myoglobin with carbon nanotube electrodes. Nanotechnology 2009;20:355502.
[11] Guo C, Hu F, Li CM, Shen PK. Direct electrochemistry of hemoglobin on carbonized titania nanotubes and its application in a sensitive reagentless hydrogen peroxide biosensor. Biosens Bioelectron 2008;24:819–24.
[12] Chakraborty S, Raj CR. Pt nanoparticle-based highly sensitive platform for the enzyme-free amperometric sensing of H_2O_2. Biosens Bioelectron 2009;24: 3264–8.
[13] Zhao W, Wang H, Qin X, Wang X, Zhao Z, Miao Z, et al. A novel nonenzymatic hydrogen peroxide sensor based on multi-wall carbon nanotube/silver nanoparticle nanohybrids modified gold electrode. Talanta 2009;80:1029–33.
[14] Shan C, Yang H, Han D, Zhang Q, Ivaska A, Niu L. Graphene/AuNPs/chitosan nanocomposites film for glucose biosensing. Biosens Bioelectron 2010;25:1070–4.
[15] Wang S, Lu L, Yang M, Lei Y, Shen G, Yu R. A novel cobalt hexacyanoferrate nanocomposite on CNT scaffold by seed medium and application for biosensor. Anal Chim Acta 2009;651:220–6.
[16] Bo X, Bai J, Wang L, Guo L. In situ growth of copper sulfide nanoparticles on ordered mesoporous carbon and their application as nonenzymatic amperometric sensor of hydrogen peroxide. Talanta 2010;81:339–45.
[17] Song MJ, Hwang SW, Whang D. Non-enzymatic electrochemical CuO nanoflowers sensor for hydrogen peroxide detection. Talanta 2010;80:1648–52.
[18] Zhang L, Li H, Ni Y, Li J, Liao K, Zhao G. Porous cuprous oxide microcubes for non-enzymatic amperometric hydrogen peroxide and glucose sensing. Electrochem Commun 2009;11:812–5.
[19] Chi Q, Dong S. Amperometric biosensors based on the immobilization of oxidases in a Prussian blue film by electrochemical codeposition. Anal Chim Acta 1995;310:429–36.
[20] Hamer M, Carballo RR, Rezzano IN. Electrocatalytic reduction of hydrogen peroxide by nanostructured bimetallic films of metalloporphyrins. Electroanalysis 2009;21:2133–8.
[21] Kumar SA, Chen S-M. Electrocatalytic reduction of oxygen and hydrogen peroxide at poly(p-aminobenzene sulfonic acid)-modified glassy carbon electrodes. J Mol Catal A Chem 2007;278:24–50.
[22] Santhosh P, Manesh KM, Gopalan A, Lee KP. Fabrication of a new polyaniline grafted multi-wall carbon nanotube modified electrode and its application for electrochemical detection of hydrogen peroxide. Anal Chim Acta 2006;575:32–8.
[23] Ghosh MK, Mittal KL. Polyimides: fundamentals & applications. New York: Marcel Dekker; 1996.
[24] Donnici CL, Filho DHM, Moreira LLC, dos Reis GT, Cordeiro ES, de Oliveira IMF, et al. Synthesis of the novel 4,4′- and 6,6′-dihydroxamic-2,2′-bipyridines and

improved routes to 4,4′- and 6,6′-substituted 2,2′-bipyridines and mono-*N*-oxide-2,2′-bipyridine. J Braz Chem Soc 1998;9:455–60.
[25] Li F, Ge JJ, Honigfort PS, Fang S, Chen J-C, Harris FW, et al. Dianhydride architectural effects on the relaxation behaviors and thermal and optical properties of organo-soluble aromatic polyimide films. Polymer 1999;40:4987–5002.
[26] Chern Y-T, Tsai J-Y. Low dielectric constant and high organosolubility of novel polyimide derived from unsymmetric 1,4-bis(4-aminophenoxy)-2,6-di-*tert*-butylbenzene. Macromolecules 2008;41:9556–64.
[27] Chern Y-T, Ju M- H. Conformation of polyimide backbone structures for determination of the pretilt angle of liquid crystals. Macromolecules 2009;42:169–79.
[28] Nakanishi K, Solomon PH. Infrared absorption spectroscopy. San Francisco: Holden Day; 1977.
[29] Tóth A, Kereszturi K, Mohai M, Bertóti I. Plasma based ion implantation of engineering polymers. Surf Coat Technol 2010;204:2898–908.
[30] Szargan R, Schaufuß A, Roßbach P. XPS investigation of chemical states in monolayers: recent progress in adsorbate redox chemistry on sulphides. J Electron Spectrosc 1999;100:357–77.
[31] Lombardi BM, Sánchez RMT, Eloy P, Genet M. Interaction of thiabendazole and benzimidazole with montmorillonite. Appl Clay Sci 2006;33:59–65.
[32] Losito I, Malitesta C, De Bari I, Calvano C-D. X-ray photoelectron spectroscopy characterization of poly(2,3-diaminophenazine) films electrosynthesised on platinum. Thin Solid Films 2005;473:104–13.
[33] Yang M, Jiang J, Lu Y, He Y, Shen G, Yu R. Functional histidine/nickel hexacyanoferrate nanotube assembly for biosensor applications. Biomaterials 2007;28:3408–17.
[34] Laviron E. Adsorption, autoinhibition and autocatalysis in polarography and in linear potential sweep voltammetry. J Electroanal Chem 1974;52:355–93.
[35] Laviron E. The use of linear potential sweep voltammetry and of a.c. voltammetry for the study of the surface electrochemical reaction of strongly adsorbed systems and of redox modified electrodes. J Electroanal Chem 1979;100:263–70.
[36] Laviron E. General expression of the linear potential sweep voltammogram in the case of diffusionless electrochemical systems. J Electroanal Chem 1979;101:19–28.
[37] Bao S-J, Li CM, Zang J-F, Cui X-Q, Qiao Y, Guo J. New nanostructured TiO_2 for direct electrochemistry and glucose sensor applications. Adv Funct Mater 2008;18:591–9.
[38] Xiao Y, Ju H-X, Chen H-Y. Direct electrochemistry of horseradish peroxidase immobilized on a colloid/cysteamine-modified gold electrode. Anal Biochem 2000;278:22–8.
[39] Thiagarajan S, Chen SM. Preparation and characterization of PtAu hybrid film modified electrodes and their use in simultaneous determination of dopamine, ascorbic acid and uric acid. Talanta 2007;74:212–22.
[40] Zhang L, Zhai Y, Gao N, Wen D, Dong S. Sensing H_2O_2 with layer-by-layer assembled Fe_3O_4–PDDA nanocomposite film. Electrochem Commun 2008;10:1524–6.